International Journal of Scientific Research in Chemical Sciences
Research Paper
Vol.4, Issue.6, pp.1-8, December (2017)
E-ISSN: 2455-3174

Investigation on Simulation of NaX Zeolite Membrane in Pervaporation process

Mansoor Kazemimoghadam*[1] and Zahra Amiri Rigi[2]

[1*]Malek Ashtar University of Technology, Faculty of Chemical and Chemical Engineering, Tehran, Iran
[2]South Tehran Branch, Islamic Azad University, Tehran, Iran

**Corresponding Author: mzkazemi@gmail.com*

Available online at: www.isroset.org

Received 22nd Mar 2017, Revised 29th Oct 2017, Accepted 5th Nov 2017, Online 30th Oct 2017

Abstract— Separation performance of Faujasite NaX zeolite membrane was studied for water-unsymmetrical dimethylhydrazine (UDMH) mixture using pervaporation (PV). A comprehensive transient model was developed using COMSOL Multiphysics software version 5.2. The developed unsteady state 2D model was capable of predicting concentration distribution in both membrane and feed phases. The membranes showed good selectivity towards water in the water-UDMH mixtures. Water permeates faster because of its preferential adsorption into the Nano-pores of the hydrophilic zeolite membrane. In PV of water-UDMH mixtures, the membrane exhibits a hydrophilic behavior, with a high selectivity towards water and a good flux. The best NaX membrane had a water flux of 2.67 kg/m2.h at 27oC. The best PV selectivity was obtained to be 40.

Keywords—Ceramics, Nanostructures, Chemical synthesis, X-ray diffraction, CFD simulation

I. INTRODUCTION

There has been an increasing interest towards zeolite membranes due to their strong potential in separation of liquid mixtures by PV. Zeolite membranes can be prepared with different methods: in situ hydrothermal synthesis; chemical vapor phase method, spray seed coating, etc. Whatever the method, an inorganic porous support is required and its nature and structure may affect the quality of the composite zeolite membrane. A popular support is made of sintered alumina. Nevertheless, this support is expensive and makes the membranes uneconomical. It is thus important to study the possibility of obtaining membranes with cheap supports. Considering its abundant resource, its low cost and its easy processing into a support with a regular structure by sintering; kaolin is a good candidate for the zeolite membranes. Zeolites X and Y is Faujasite-type molecular sieve with high aluminum content that possesses a three dimensional channel structure with equi-dimensional channels intersecting in a perpendicular fashion with 0.74 nm free apertures.

Many studies have been carried out to simulate mass transfer through PV membranes [8, 23-29]. In pervaporation, the feed mixture is contacted with a nonporous perm selective membrane. Separation is, in general, explained by the steps of sorption into, diffusion through and desorption from the membrane. The latter is usually considered to be fast and taking place at equilibrium, while diffusion is kinetically controlled and the slowest step of the process. Permeation is dependent on sorption and diffusion steps. The driving force for the separation is created by maintaining a pressure lower than the saturation pressure on the permeate side of the membrane. The mechanism of separation is usually explained in terms of sorption-diffusion processes. Mass transfer through PV membranes is usually described by the equations of mass and momentum conservation (Navier-Stokes equations). Modeling based on solving these equations with finite element method (FEM) is previously used to describe concentration distribution in PV systems [23, 24]. Based on this method, Moulik et al. proposed a steady state model to predict mass transfer of MMH and UDMH solutions by pervaporation [23]. Their results were in good agreement with experimental data. However, their model was not comprehensive, since they only modeled the membrane section of the module and also assumed the conditions to be steady state. As understood, a complete transient model is essential that is capable of modeling membrane section as well as feed compartment.

In this paper, a comprehensive unsteady state model was finally developed using COMSOl Multiphysics software version 5.2. Effect of various feed flow rates, membrane lengths and widths were investigated to find the optimum operating conditions. The developed model was capable of

predicting concentration distribution of water in both membrane and the feed phases.

II. EXPERIMENTAL

In this study, several zeolite membranes prepared in previous studies were used. Molar composition of the starting gel of the NaX zeolite membranes were SiO_2/Al_2O_3=2.5-4, Na_2O/SiO_2=1.08-2, H_2O/Na_2O=30-200 [31-33].

The zeolite membranes were used for dehydration of water/UDMH mixtures. Experiments were carried out at a temperature of 30°C and a pressure of 1.5 mbar at the permeate side, within a period of 30-60 min. The final membrane used for PV experiments had 44 cm^2 surface area, 12 cm length, 5 mm inner radius and 5.835 mm outer radius. The feed solution flowed over the outer surface of the membrane module and the permeate water was collected from the inner part of that.

Permeate concentrations were measured using GC (TCD detector, Varian 3400, carrier gas: hydrogen, column: polyethylene glycol, sample size: 5 μm, column and detector temperatures: 120-150°C, detector flow: 15 ml/min, carrier flow: 5 ml/min, column pressure: 1.6 kpa, GC input pressure: 20 kpa). Performance of PV was evaluated using values of total flux ($kg/m^2.h$) and separation factor (dimensionless). While PV system was at steady state (after 20 min), weight of permeate was measured at 30 min period and then flux was calculated (surface area of the zeolite membrane was 44 cm^2). The change in feed concentration due to permeation was negligible because the amount of permeate was small (max 2 ml) compared with total liquid volume in the system (0.5 lit). A three stage diaphragm vacuum pump (vacuubrand, GMBH, Germany) was employed to evacuate the permeate side of the membrane to a pressure of approximately 1.5 mbar while the feed side was kept at atmospheric pressure. The permeate side was connected to a liquid nitrogen trap via a hose to condense the permeate (vapor) (Fig. 1).

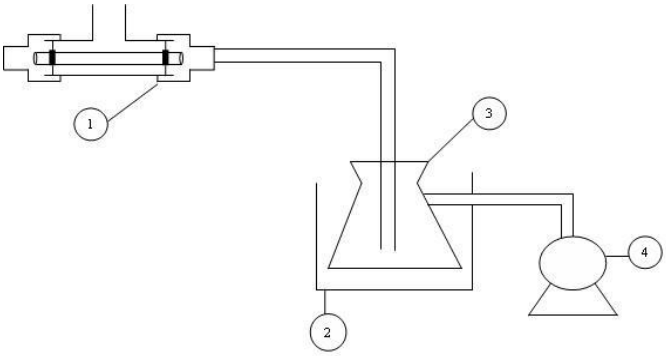

Fig. 1 PV setup; 1- feed container and PV cell 2- liquid nitrogen trap 3- permeate container 4- three stage vacuum pump

Table 1 Flux and separation factor of the Nano pore faujasite zeolite membranes

NO	Zeolite type	SiO_2/Al_2O_3	Na_2O/Al_2O_3	H_2O/Al_2O_3	t (h)	T (°C)	Flux $kg/m^2.h$	Separation factor
1	NaX	3.25	5	150	6	100	2.0	26
2	NaX	3.25	3.5	150	6	100	2.67	15
3	NaX	3.25	6.5	150	6	100	2.60	10
4	NaX	2.5	5	150	6	100	2.0	15
5	NaX	3.25	5	150	6	100	2.0	26
6	NaX	4	5	150	6	100	2.34	40

III. MODELING

Fig. 2 represents the schematic diagram of the model domain used in the simulation. Feed solution containing a mixture of 5 wt. % UDMH and 95 wt. % water flows tangentially through the upper side of the membrane system (z=0) and exits at z=L.

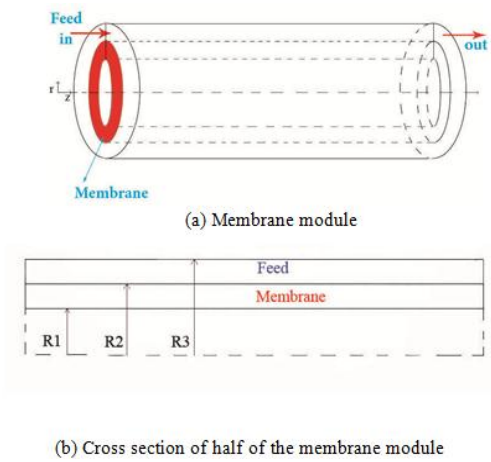

Fig. 2 Model domain used in the simulation; (a) Membrane module and (b) cross section of half of the membrane module

The main assumptions to develop the numerical simulation are as follows:

- Time dependent conditions.
- Temperature is constant.
- No chemical reaction occurs in feed stream.
- Feed solution flows only in the z direction.
- Laminar feed flow in the membrane system.
- Thermodynamic equilibrium considered at the interface of feed and membrane.
- Small amount of UDMH permeates through the membrane.
- Mass transfer resistance of the support layer was assumed to be negligible.
- Fouling and concentration polarization effects on the PV of UDMH solution are negligible.
- Feed viscosity and density are constant.

Axial and radial diffusions inside the membrane and feed phase are considered in the continuity equations. Moreover, small permeation of UDMH through the membrane is

considered in the simulation by applying selectivity equation (Eq. (1)). The penetration of UDMH through the selective membrane is described by the following equation:

$$S = \frac{x_{UDMH}}{x_{water}} \times \frac{y_{water}}{y_{UDMH}} \quad (1)$$

The concentration of UDMH in the permeate side (y_{UDMH}) must be determined by trial and error method. In this method, an initial value for y_{UDMH} is guessed. Then the water concentration in the permeate side is calculated using model equations. This calculated value then is compared with the guessed value. If the difference between the old and new values is less than a determined error, the guessed UDMH concentration is considered as the correct concentration. Otherwise, another guess must be made for y_{UDMH}.

Mass transport in the membrane system is described using continuity equation. The following equation presents the differential form of this equation [34]:

$$\frac{\partial C_{water}}{\partial t} + \nabla.(-D_{water}\nabla C_{water} + U.C_{water}) = R \quad (2)$$

where C_{water} denotes water concentration (mol/m^3), D_{water} denotes water diffusion coefficient (m^2/s), U denotes the velocity vector (m/s) and R denotes the reaction term (mol/m^3.s). Since no chemical reactions take place in UDMH/water PV, the reaction term is zero. Continuity equation was defined and solved in COMSOL Multiphysics 5.2 by adding a "transport of diluted species" physic to the model. Velocity distribution was obtained by solving Navier-Stokes equation for momentum balance, simultaneously with continuity equation in the feed side. This was done by adding a "laminar flow" physic to the whole model in COMSOL Multiphysics 5.2. The following equation describes the momentum conservation equation [34]:

$$\rho\frac{\partial u}{\partial t} + \rho(u.\nabla)u = \nabla.[-P + \mu(\nabla u + (\nabla u)^T)] + F \quad (3)$$

$$\nabla.(u) = 0 \quad (4)$$

Where u denotes z-component of velocity vector (m/s), ρ denotes feed density (kg/m^3), P denotes pressure (Pa), μ denotes feed viscosity (Pa.s) and F denotes a body force (N).

Feed phase simulation

By applying mentioned assumptions to the Eq. (2), unsteady state form of the continuity equation for water mass transport in the feed side is obtained:

$$\frac{\partial C_{water}}{\partial t} - \frac{1}{r}\frac{\partial}{\partial r}\left(D_{water} r \frac{\partial C_{water}}{\partial r}\right) - \frac{\partial}{\partial z}\left(D_{water}\frac{\partial C_{water}}{\partial z}\right) + u\frac{\partial C_{water}}{\partial z} = 0 \quad (5)$$

The simplified form of the momentum transport equations considering above assumptions will be as follows:

$$\rho\left(\frac{\partial u}{\partial t} + u\frac{\partial u}{\partial z}\right) - \frac{1}{r}\frac{\partial}{\partial r}\left(r\mu\frac{\partial u}{\partial r}\right) - \frac{\partial}{\partial z}\left(\mu\frac{\partial u}{\partial z}\right) = -\frac{\partial P}{\partial z} \quad (6)$$

$$\frac{\partial u}{\partial z} = 0 \quad (7)$$

where r and z denote radial and axial coordinates, respectively.

The initial conditions for mass and momentum conservation equations are as follows:

at t=0, $C_{water\text{-}feed}=C_{0,water}$ and $u=u_0$ (8)

where $C_{water\text{-}feed}$ is water concentration in feed phase, $C_{0,water}$ is its initial value and u_0 is initial velocity of feed flow.

The boundary conditions for mass conservation equations in feed phase are as follows:

at z=L, Outflow condition (9)

at z=0, $C_{water\text{-}feed}=C_{0,water}$ (Inlet boundary) (10)

at r=R_3, Symmetry (11)

At the interface of membrane-feed, the equilibrium condition is assumed:

at r= R_2, $C_{water-feed} = \frac{C_{water-membrane}}{n}$ (12)

in which $C_{water\text{-}membrane}$ is water concentration in membrane section and n is partition coefficient obtained from selectivity equation as follows:

$$n = \frac{y_{UDMH}}{x_{UDMH}} \times S = \frac{C_{water-membrane}}{C_{water-feed}} \quad (13)$$

As mentioned earlier, permeate concentration of UDMH obtained using trial and error method, and then was placed in the above equation.

The boundary conditions for momentum transfer equations are as follows:

at z=0, u=u_0, (Inlet boundary) (14)

At the outlet, the pressure is atmospheric pressure:

at z=L, P=P_{atm}, (Atmospheric pressure) (15)

at r=R_2 , u=0 (No slip (16)

condition)

at $r=R_3$, Symmetry (17)

Membrane phase simulation

Mass transport of water in membrane is controlled only by diffusion mechanism. Therefore, the unsteady state continuity equation for water can be written as:

$$\frac{\partial C_{water-membrane}}{\partial t} - \frac{1}{r}\frac{\partial}{\partial r}\left(D_{membrane}\, r \frac{\partial C_{water-membrane}}{\partial r}\right) - \frac{\partial}{\partial z}\left(D_{membrane}\frac{\partial C_{water-membrane}}{\partial z}\right) = 0 \quad (18)$$

where $D_{membrane}$ is water diffusion coefficient in membrane (m^2/s).

Membrane phase boundary conditions are given as:

at $r=R_2$, $C_{water-membrane} = n \times C_{water-feed}$ (Equilibrium condition) (19)

at $r= R_1$, $C_{water-membrane}=0$ (Dry membrane condition) (20)

at z=0 and z=L, $\frac{\partial C_{water-membrane}}{\partial z} = 0$ (No flux condition) (21)

At the permeate-membrane interface, water concentration assumed to be zero due to the vacuum applied.

Numerical solution of conservation equations

Set of model equations, including mass and momentum transfer equations in the membrane module along with suitable boundary conditions was solved using COMSOL Multiphysics software version 5.2. Finite element method (FEM) was used by this software to solve conservation equations numerically. The computational time for solving the equations was 518s. "Extra fine mesh" used for meshing in this simulation. Complete mesh consisted of 70489 domain elements and 1944 boundary elements for solving the set of equations. Number of degrees of freedom was 115153 (plus 3143 internal DOFs). Fig. 3 represents the meshes was created by COMSOL Multiphysics 5.2 software. Due to considerable difference between z and r dimensions, a scaling factor equal to 6 was used in z direction. Therefore, the results were reported in dimensionless length.

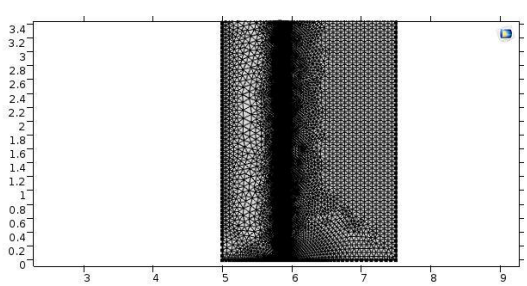

Fig. 3 Magnified segments of the mesh generated by COMSOL; Complete mesh consists of 70489 domain elements

IV. RESULTS AND DISCUSSION

Water concentration distribution in feed phase

Fig. 4 shows the concentration distribution of water in feed phase at different separation times. The UDMH/water solution containing 95 wt. % water flows over the outer surface of the membrane module (z=0). As can be seen from the figure, a concentration boundary layer is formed at the beginning of the separation process. Over an extended period of time, thickness of this layer increases. At z=0, the water concentration is maximum (95 wt. %). As the feed solution flows in the feed compartment, water moves towards the membrane surface due to the concentration and pressure differences (driving forces). Therefore, the water concentration on the membrane surface is less than its value at feed inlet (where water concentration is equal to its initial value, $C_{0,\ water}$). The water concentration on the membrane surface was calculated by the membrane selectivity (Eq. 12) and its value in the membrane side. Since water concentration in membrane is always less than its value in feed, the water concentration on membrane-feed boundary ($r=R_2$) is always less than its value in feed bulk. At the feed outlet (z=L) water concentration is minimum, as expected. Over a longer period of separation time, minimum water concentration in concentrate part (feed part) decreases due to the water diffusion through the membrane.

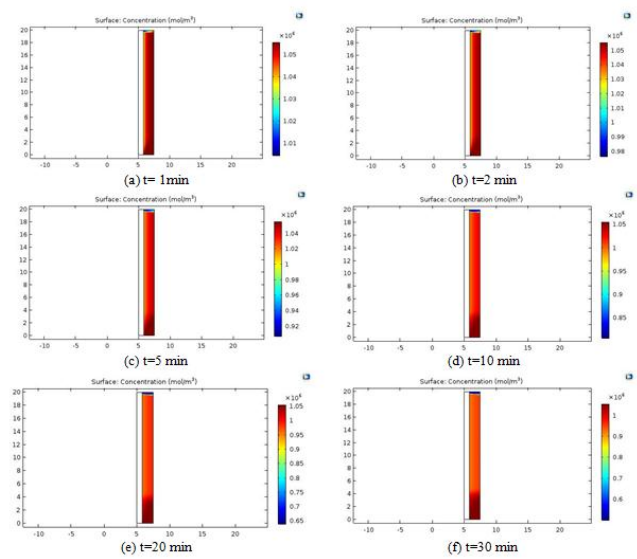

Fig. 4 Concentration distribution of water in feed phase ($C_{water-feed}$) at different separation times (1 l/min flow rate and 30°C temperature); (a) 1min, (b) 2min, (c) 5min, (d) 10min, (e) 20min and (f) 30min

Fig. 5 presents the water concentration in the feed phase versus r-coordinate at different lengths and times. Water concentration increases along r direction, as expected. The concentration gradient is great at regions near the membrane-feed interface ($r=R_2$) due to the mass transfer towards the membrane at this region. Over a longer period of time, total water concentration decreases due to mass transfer towards

the membrane. Change in total concentration vs. r-coordinate is negligible up to 90mm membrane lengths at a specified separation time. However, at the regions near the feed outlet the concentration decreased considerably. The concentration gradient along r direction also decreased at this region. This can be attributed to lower water concentrations in regions near z=L compared to feed inlet, as mentioned before, which reduces the driving force (concentration gradient). Over an extended period of time, total concentration decreased due to mass transfer through the membrane.

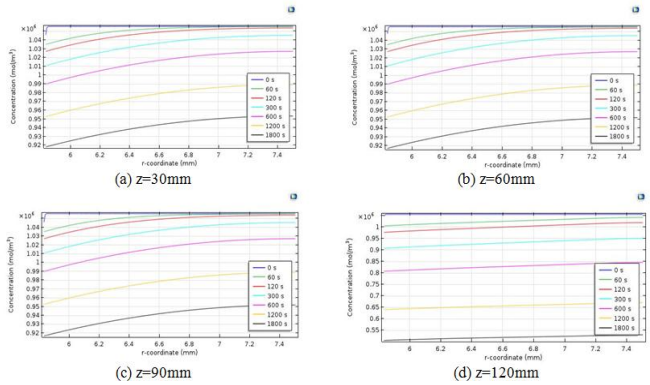

Fig. 5 Concentration distribution of water in feed phase ($C_{water\text{-}feed}$) vs. radius at various membrane lengths (1 l/min flow rate and 30°C temperature); (a) 30mm, (b) 60mm, (c) 90mm and (d) 120mm

Fig. 6 demonstrates the concentration distribution along z coordinate at constant flow rate (1 l/min) and different radii. Results show that the variation of water concentration along the z coordinate is considerable (about 10% at 1800s) and cannot be neglected compared to its variation along r coordinate. The figure also indicates that the concentration gradient near the membrane-feed interface ($r=R_2$) is greater, while is less and also delayed at greater radii. This behavior can be attributed to water transfer towards the membrane at this region. Concentration variation increases over an extended period of time. Thus, time-dependent study is necessary in PV simulations and the stationary condition which was assumed by previous studies is not a good assumption [23, 24].

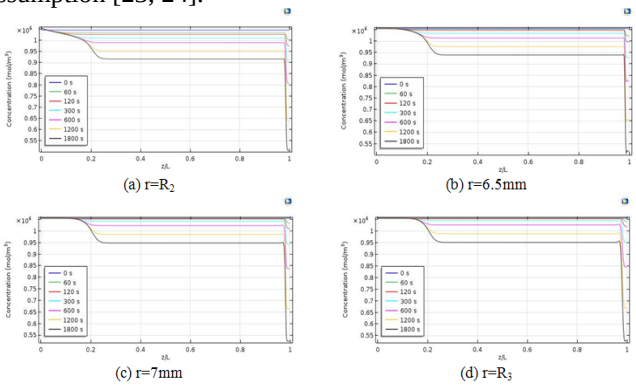

Fig.6 Water concentration distribution in feed phase vs. dimensionless length (1 l/min flow rate and 30°C temperature) at various radii; (a) $r=R_2$, (b) r=6.5mm, (c) r=7mm and (d) $r=R_3$

Figs. 7 and 8 show the effect of various feed flow rates (0.5, 1 and 1.5 l/min) on water concentration along z and r directions, respectively. At greater values of feed flow rate, water concentration values are greater (at the same radius or dimensionless length), because an increase in feed flow rate, diminishes the contact time of feed flow with membrane, thus less water has enough time to pass through the membrane. This is in good agreement with what is expected in real conditions.

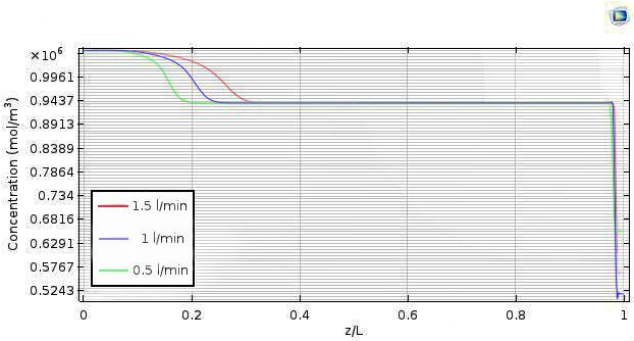

Fig.7 Water concentration distribution vs. dimensionless length in feed phase at 30°C temperature and various feed flow rates

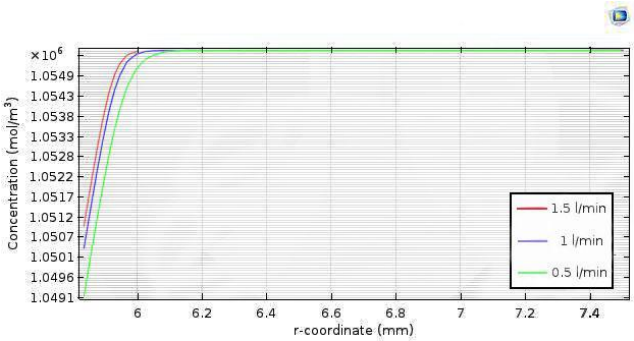

Fig.8 Water concentration distribution in feed phase vs. radius at 30°C temperature and various feed flow rates

Water concentration distribution in membrane phase

Fig. 9 shows the concentration distribution of water in membrane phase at different separation times. Water transfer through the membrane was described only by diffusion mechanism. Since at the membrane-permeate interface the vacuum condition was assumed, the water concentration on this boundary is zero at all separation times. Water concentration is highest on the membrane-feed interface, because the water concentration on this boundary is calculated from its value in the feed section, which is highest at the beginning of the separation process. Over a longer period of time however, water concentration at the membrane length (z=L) decreases, due to the concentration decrease in feed side (as mentioned in the previous section). These results are very close to what happens in real conditions.

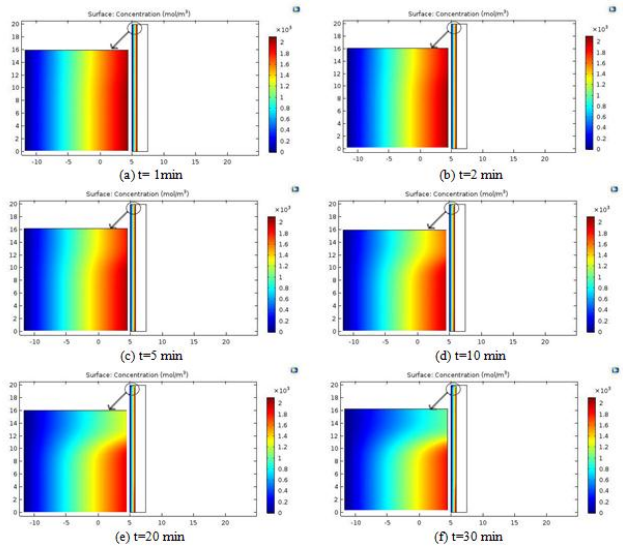

Fig.9 Concentration distribution of water in membrane phase ($C_{water\text{-}membrane}$) at different separation times (1 l/min flow rate and 30°C temperature); (a) 1min, (b) 2min, (c) 5min, (d) 10min, (e) 20min and (f) 30min

Fig. 10 presents the water concentration in the membrane phase versus r-coordinate at different lengths and times. Water concentration increases with radius, as expected. Concentration value on the membrane-feed boundary ($r=R_2=5.835$mm) is maximum at any time, because it is calculated from water concentration in feed side, where its value is maximum. On the membrane-permeate interface, water concentration is zero because of vacuum applied in permeate side (dry membrane condition). The concentration gradient profile is almost the same at membrane lengths up to 90mm. However, in regions near the membrane length (z=120mm), concentration gradient decreases over an extended period of time. This is because the model considers loss of concentration in this region and longer periods of time, due to more water transfer towards the membrane at regions near the feed inlet. As seen, the developed model powerfully is capable of predicting this mass loss at z=L and different separation times, which was neglected in previous studies [23].

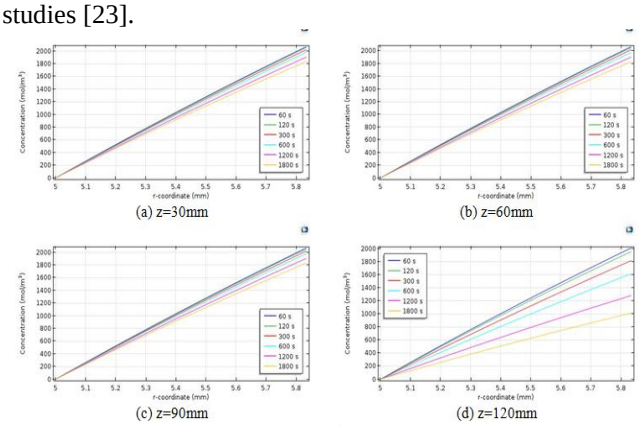

Fig. 10 Concentration distribution of water in membrane phase ($C_{water\text{-}membrane}$) at different membrane lengths (1 l/min feed flow rate and 30°C temperature); (a) 30mm, (b) 60mm, (c) 90mm and (d) 120mm

Fig. 11 demonstrates the concentration distribution vs. dimensionless length at constant flow rate (1 l/min) and different membrane radii. Results show that the variation of water concentration along the z coordinate at constant radius is considerable and cannot be neglected compared to its variation along r coordinate. Its variation is also greater over an extended period of time, as expected. The total shape of concentration distribution is almost the same at various radii. However, at radii far from the membrane-permeate interface, the concentration increases considerably. This is because water concentration on the membrane-feed interface is calculated from selectivity equation (Eq. 19) and water concentration in feed phase, where its value is highest.

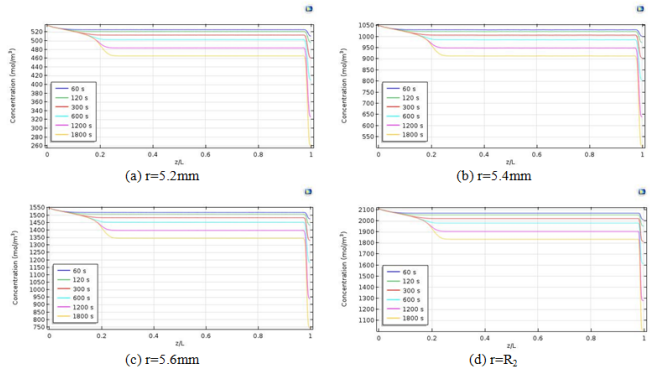

Fig. 11 Concentration distribution of water in membrane phase ($C_{water\text{-}membrane}$) vs. dimensionless length at different radii (1 l/min flow rate and 30°C temperature); (a) r=5.2mm, (b) r=5.4mm, (c) r=5.6mm and (d) $r=R_2$

Fig. 12 shows the effect of various feed flow rates (0.5, 1 and 1.5 l/min) on water concentration along the z coordinate. As can be seen from the figure, water concentration is higher at greater flow rates. This is because an increase in feed flow rate diminishes the contact time of feed flow with membrane. Thus higher concentrations are achieved in the feed phase and consequently in the membrane (according to Eq. 19). However, concentration distribution is almost the same at lengths more than 30mm.

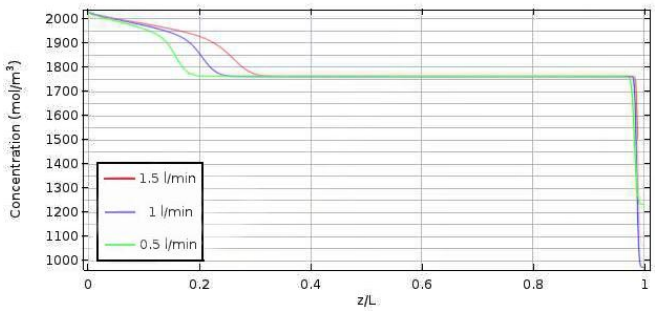

Fig. 12 Concentration distribution of water in membrane phase ($C_{water\text{-}membrane}$) vs. dimensionless length at different feed flow rates

Velocity distribution in feed phase

Fig. 13 shows the velocity field in the feed phase of the PV membrane system. The velocity distribution was obtained using numerical solution of momentum balance. This was done by adding a "laminar flow" physic to the whole model

in COMSOL. As can be seen from the figure, the velocity profile is fully developed at the feed phase. Velocity is zero on the membrane-feed interface due to no slip conditions assumed on this boundary and is highest on the right side of the feed section due to symmetry boundary condition.

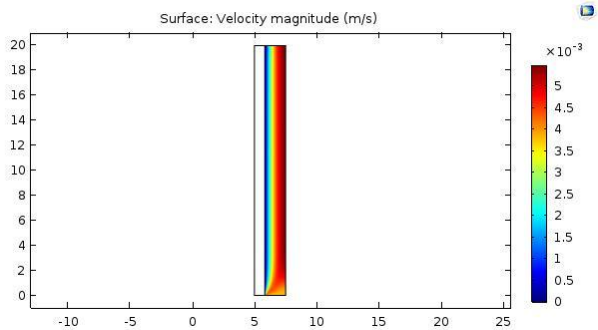

Fig. 13 Velocity distribution in the feed phase at 1 l/min feed flow rate and 30°C temperature

Fig. 14 shows the velocity profile vs. radius in half of the membrane module. As can be seen, the velocity profile is parabolic and becomes fully developed after a short distance (lengths more than 12mm). As seen, entrance effects are considered in this simulation.

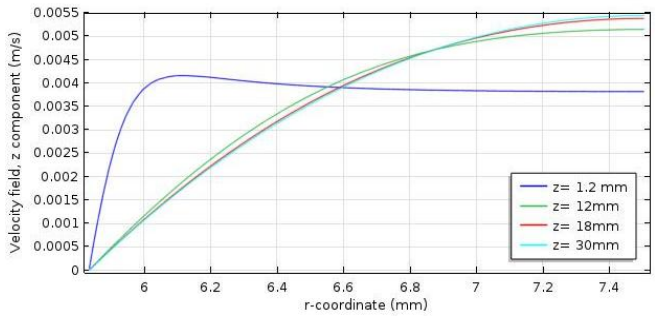

Fig. 14 Velocity profile vs. r-coordinate at various membrane lengths (1 l/min feed flow rate and 30°C temperature)

Fig. 15 represents velocity distribution vs. dimensionless length. Velocity profile is almost parabolic and reaches its maximum value at the regions close to feed entrance. The maximum velocity is greater at higher feed flow rates, as expected.

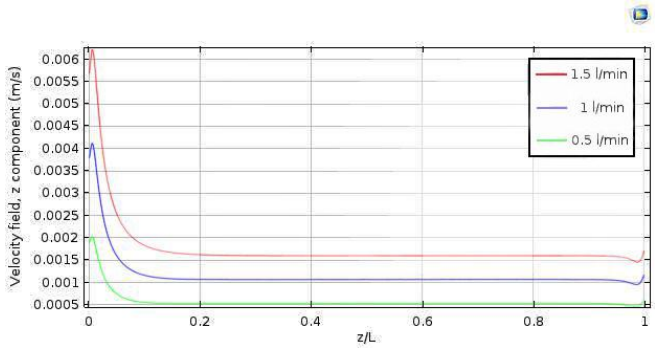

Fig. 15 Velocity profile vs. dimensionless length at different feed flow rates

V. CONCLUSION

Zeolite membranes showed much higher fluxes and separation factors than commercially available polymeric membranes. These membranes showed good membrane performance for separation of the UDMH-water mixtures. It is expected that even significantly higher fluxes, with similar separation factors, can be achieved at higher temperatures. It was found that PV using NaX zeolite membranes is an effective technique to separate water from the water-UDMH mixtures. A comprehensive unsteady state model was also developed for the pervaporation of water-UDMH mixture. Effect of various feed flow rates, membrane lengths and widths was investigated to find the optimum separation conditions. The developed model was powerfully capable of predicting concentration and velocity distributions in the membrane module.

Nomenclature

C_{water}	water concentration (mol/m^3)
$C_{0,water}$	initial water concentration (mol/m^3)
$C_{water\text{-}feed}$	water concentration in feed (mol/m^3)
$C_{water\text{-}membrane}$	water concentration in membrane (mzol/m^3)
D_{water}	water diffusion coefficient (m^2/s)
$D_{membrane}$	water diffusion coefficient in membrane (m^2/s)
F	body force (N)
L	membrane length (mm)
n	partition coefficient
P	pressure (Pa)
P_{atm}	atmospheric pressure (Pa)
r	radial coordinate
R_1	permeate-membrane radius (mm)
R_2	membrane-feed radius (mm)
R_3	feed outer radius (mm)
R	reaction term (mol/m^3.s)
S	selectivity
t	separation time (s)
U	velocity vector (m/s)
u	z-component velocity (m/s)
x_{UDMH}	UDMH wt.% in feed
x_{water}	water wt.% in feed
y_{UDMH}	UDMH wt.% in permeate
y_{water}	water wt.% in permeate
z	axial coordinate
ρ	density (kg/m^3)
μ	viscosity (Pa.s)

REFERENCES

[1] S. Hu, W. Ren, D. Cai, T. C. Hughes, P. Qin, T. Tan, A mixed matrix membrane for butanol pervaporation based on micron-sized

silicalite-1 as macro-crosslinkers, Journal of Membrane Science 533 (2017) 270–278.
[2] Q. Wang, N. Li, B. Bolto, M. Hoang, Z. Xie, Desalination by pervaporation: A review, Desalination 387 (2016) 46-60.
[3] J. Li, N. Wang, H. Yan, G. Zhang, Z. Qin, S. Ji, G. Zhang, Roll-coating of defect-free membranes with thin selective layer for alcohol perm-selective pervaporation: From laboratory scale to pilot scale, Chemical Engineering Journal 289 (2016) 106-113.
[4] Y.M. Xu, T.S. Chung, High-performance UiO-66/polymide mixed matrix membranes for ethanol, isopropanol and n-butanol dehydration via pervaporation, Journal of membrane Science 531 (2017) 16-26.
[5] W.F. Yong, P. Salehian, L. Zhang, T.S. Chung, Effects of hydrolyzed PIM-1 in polymide-based membranes on C_2-C_4 alcohols dehydration via pervaporation, Journal of Membrane Science 523 (2017) 430-438.
[6] Y.M. Xu, N.L. Le, J. Zuo, T.S. Chung, Aromatic polymide and crosslinked thermally rearranged poly (benzoxazole-co-imide) membranes for isopropanol dehydration via pervaporation, Journal of Membrane Science 499 (2016) 317-325.
[7] M. Fathizadeh, A. Aroujalian, A. Raisi, M. Fotouhi, Preparation and characterization of thin film nanocomposite membrane for pervaporation dehydration of aqueous alcohol solutions, Desalination 314 (2013) 20-27.
[8] M. Samei, M. Iravaninia, T. Mohammadi, A.A. Asadi, Solution diffusion modeling of a composite PVA/fumed silica ceramic supported membrane, Chemical Engineering and Processing: Process Intensification 109 (2016) 11-19.
[9] A.A. Kittur, S.S. Kulkarni, M.I. Aralaguppi, M.Y. Kariduraganavar, Preparation and characterization of novel pervaporation membranes for the separation of water–isopropanol mixtures using chitosan and NaY zeolite, Journal of Membrane Science 247(1-2) (2005) 75–86.
[10] M.Y. Kariduraganavar, A.A. Kittur, S.S. Kulkarni, K. Ramesh, Development of novel pervaporation membranes for the separation of Water–isopropanol mixtures using sodium alginate and NaY zeolite, Journal of Membrane Science 238(1-2) (2004) 165–175.
[11] C.H. Cho, K.Y. Oh, J.G. Yeo, S.K. Kim, Y.M. Lee, Synthesis, ethanol dehydration and thermal stability of NaA zeolite/alumina composite membranes with narrow non-zeolitic pores and thin intermediate layer, Journal of Membrane Science 364(1-2) (2010) 138-148.
[12] H. Kita, K. Fuchida, T. Horita, H. Asamura, K. Okamoto, Preparation of Faujasite membranes and their permeation Properties, Separation and Purification Technology 25(1-3) (2001) 261–268.
[13] S.G. Sorenson, E.A. Payzant, W.T. Gibbons, B. Soydas, H. Kita, R.D. Noble, J.L. Falconer, Influence of zeolite crystal expansion/contraction on NaA zeolite membrane Separations, Journal of Membrane Science 366(1-2) (2011) 413–420.
[14] R. Ravindra, S. Sridhar, A.A. Khan, A.K. Rao, Pervaporation of water, hydrazine and monomethylhydrazine using ethyl cellulose membranes, Polymer 41(8) (2000) 2795-2806.
[15] S. Sridhar, R. Ravindra, A.A. Khan, Recovery of monomethylhydrazine liquid propellant by pervaporation technique, Ind.Eng.Chem. Res. 39(7) (2001) 2485-2490.
[16] X. Li, I. Kresse, Z.K. Zhou, J. Springer, Effect of temperature and pressure on gas transport in ethyl cellulose membrane, Polymer 42(16) (2001) 6801-6810.
[17] R. Ravindra K.R. Krovvidi, A.A. Khan, A.K. Rao, D.S.C. studies of states of water, hydrazine and hydrazine hydrate in ethyl cellulose membrane, Polymer 40(5) (1999) 1159-1165.
[18] R. Ravindra, A. Kameswara, A. Khan, A qualitative evaluation of water and monomethyl hydrazine in ethyl cellulose membrane, Journal of Applied Polymer Science 72 (1999) 689-700.
[19] S. Sridhar, G. Susheela, G.J. Reddy, A.A. Khan, Cross linked chitosan membranes: characterization and study of dimethylhydrazine dehydration by pervaporation, Polymer International 50(10) (2001) 1156-1165.
[20] R. Ravindra, A.K. Rao, A.A. Khan, Processing of liquid propellant reaction liquors by pervaporation, Journal of Applied Polymer Science 72(1) (1999) 141-149.
[21] R. Ravindra, S. Sridhar, A.A. Khan, Separation studies of hydrazine from aqueous Solutions by Pervaporation, Journal of Polymer Science: Part B: Polymer Physics 37(16) (1999) 1969-1980.
[22] R. Ravindra, R. Krovvidi, A.A. Khan, Solubility parameter of chitin and chitosan, Carbohydrate Polymers 36(2-3) (1998) 121-127.
[23] S. Moullik, K.P. Kumar, S. Bohra, S. Sridhar, Pervaporation performance of PPO membranes in dehydration of highly hazardous MMH and UDMH liquid propellants, Journal of Hazardous Materials 288 (2015) 69-79.
[24] M. Rezakazemi, M. Shahverdi, S. Shirazian, T. Mohammadi, A. Pak, CFD simulation of water removal from water/ethylene glycol mixtures by pervaporation, Chemical Engineering Journal 168(1) (2011) 60-67.
[25] A. Rom, A. Miltner, W. Wukovits, A. Friedl, Energy saving potential of hybrid membrane and distillation process in butanol purification: Experiments, modeling and simulation, Chemical Engineering and Processing 104 (2016) 201-211.
[26] D. Liu, G. Liu, L. Meng, Z. Dong, K. Huang, W. Jin, Hollow fiber modules with ceramic-supported PDMS composite membranes for pervaporation recovery of bio-butanol, Separation and Purification Technology 146 (2015) 24-32.
[27] M. Jain, D. Attarde, S.K. Gupta, Removal of thiophenes from FCC gasoline by using a hollow fiber pervaporation module: Modeling, validation and influence of module dimensions and flow directions, Chemical Engineering Journal 308 (2017) 632-648.
[28] S. Moulik, S. Nazia, B. Vani, S. Sridhar, Pervaporation separation of acetic acid/water mixtures through sodium alginate/polyaniline polyion complex membrane, Separation and Purification Technology 170 (2016) 30-39.
[29] Z. Qiao, Y. Wu, X. Li, J. Zhou, Molecular simulation on the separation of water/ethanol azeotropic mixture by poly(vinyl alcohol) membrane, Fluid Phase Equilibria 302(1-2) (2011) 14-20.
[30] M. Kazemimoghadam, A. Pak, T. Mohammadi, Dehydration of water/1-1-dimethylhydrazine mixtures by zeolite membranes, Microporous and Mesoporous Materials 70(1-3) (2004) 127-134.
[31] Z. Xu, Q. Chen, G. Lu, Preparation of Zeolite X Membranes on Porous Ceramic Substrates with Zeolite Seeds, Journal of Natural Gas Chemistry 11 (2002)171-179.
[32] S. Li, V.A. Tuan, J.L. Falconer, R.D. Noble, X-type zeolite membranes: preparation, characterization, and pervaporation performance, Microporous and Mesoporous Materials 53(1-3) (2002) 59-70.
[33] G.M. Johnson, Y. Lee, A. Tripathi, J.B. Parise, Structural studies of hydrated germanium X-type zeolite via Rietveld analysis of synchrotron powder X-ray diffraction data, Microporous and Mesoporous Materials 31(1-2) (1999) 195-204.
[34] R.B. Bird, W.E. Stewart, E.N. Lightfoot, Transport phenomena, John Wiley & Sons, New York, 2nd edition, (1960) 780.

